Rheologica Acta Rheol Acta 31:592–602 (1992)

An analytical solution for the temperature profiles during injection molding, including dissipation effects

K. M. B. Jansen and J. van Dam

Department of Polymer Technology, Delft University of Technology, Delft, The Netherlands

Abstract: An analytical solution is obtained for the stationary temperature profile in a polymeric melt flowing into a cold cavity, which also takes into account viscous heating effects. The solution is valid for the injection stage of the molding process. Although the analytical solution is only possible after making several (at first sight) rather stringent assumptions, the calculated temperature field turns out to give a fair agreement with a numerical, more realistic approach. Approximate functions were derived for both the dissipation-independent and the dissipation-dependent parts which greatly facilitate the temperature calculations. In particular, a closed-form expression is derived for the position where the maximum temperature occurs and for the thickness of the solidified layer.

The expression for the temperature field is a special case of the solution of the diffusion equation with variable coefficients and a source term.

Key words: Injection molding; viscous dissipation; solidified layer; diffusion equation

Nomenclature

a	$\dfrac{\lambda}{\varrho c}$, thermal diffusivity [$m^2/s$]
c	specific heat [J/kg K]
D	channel half-height [m]
L	channel length [m]
m	$1/\nu$
P	pressure [Pa]
T	temperature [°C]
T_w	wall temperature [°C]
T_i	injection temperature [°C]
T_A	Br independent part of T
T_B	Br dependent part of T
T^{core}	asymptotic temperature
$v_z(x)$	axial velocity [m/s]
W	channel width [m]
x	cross-channel direction [m]
z	axial coordinate [m]
$\Gamma(x)$	gamma function
$\gamma(a,x)$	incomplete gamma function
$M(a,b,x)$	Kummer function
ε	small parameter
$\vartheta(\chi)$	temperature function
λ	thermal conductivity [W/mK]
μ	viscosity [Pa·s]
μ_0	consistency index
ν	power-law exponent
ϱ	density [kg/m]
χ	similarity variable

Dimensionless variables

$$\text{Br} = \frac{\mu_0 D^2}{\lambda (T_i - T_w)} \left(\frac{(m+2)\langle v_z \rangle}{D} \right)^{(m+1)/m},$$

Brinkman number

$$\text{Gz} = \frac{\langle v_z \rangle D^2}{aL},$$ Graetz number

$$\tilde{T} = \frac{T - T_w}{T_i - T_w}$$

$\tilde{v}_z = v_z/\langle v_z \rangle$
$\tilde{x} = x/D$
$\hat{x} = 1 - \tilde{x}$
$\tilde{z} = z/L$

1. Introduction

Injection molding is a widely used cyclic process by which the raw polymer material is shaped into a product of the desired form. During this process the solid polymer is melted, forming a hot liquid which is injected into a cold mold. In the mold the melt is cooled and solidified. After the filling stage, some additional melt is injected as a compensation for the thermal shrinkage of the solidifying polymer.

The combined effect of flow and cooling results in an orientation distribution which varies downwards from the product surface to the core (Wales 1972). This orientation distribution influences the mechanical and optical properties of the product. Since the relaxation times of the oriented polymer molecules strongly depend on the temperature, a detailed knowledge of the temperature profiles is crucial for a good understanding of the relaxation processes.

In this paper the temperature development is studied with an emphasis on the region near the mold walls where the largest orientation levels are created. As the trend in industry today is to molding at moderate to high injection speeds, only those situations are considered where the ratio of heat convection to heat conduction is large ($Gz > 50$).

A review of the solutions of the problems concerning the cooling of a flowing viscous melt is given by Pearson (1985). Perturbation solutions without the viscous dissipation effects were first obtained by Lévêque (1928) and Newman (1969). It is clear that in the case of large flow rates heating by dissipation can no longer be disregarded. A first term approximation of the viscous heating contribution was presented by Richardson (1979, 1983). However, this solution tends to give too high an estimate of the temperatures in situations where $Gz = 0(100)$ and the viscous dissipation is high ($Br > 10$), corresponding to common injection molding conditions. In the present paper a more extended expression for the viscous dissipation part will be derived, the first term of which corresponds with Richardson's solution. The solution presented here agrees quite well with numerical solutions. It also converges to the solution valid for the region far from the wall and is thus able to describe the maximum temperature due to viscous heating.

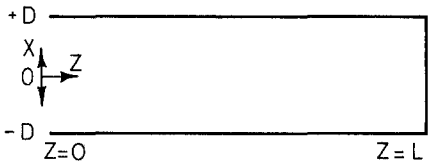

Fig. 1. Schematic representation of the mold

2. Theory

The description given here will be restricted to the most simple mold geometry, a long, thin rectangular cavity equipped with a film gate (see Fig. 1). As is shown by Richardson (1979), only minor changes are required to adapt the solution for a rectangular geometry to other geometries. Furthermore, solutions for film-gated cavities can be transformed into solutions for cavities with a point gate (Ryan and Chung 1980). The effect of the solidifying layer on the velocity profile will be disregarded. In general, this effect is small; if this is not the case the solution may easily be extended as indicated by Richardson (1983).

In polymer melt flow the temperature distribution is influenced by the velocity distribution and vice versa. As a consequence the momentum and energy equations are coupled and, due to mathematical complications, a complete solution can only be obtained by numerical simulation. However, an analytical solution which retains most of the relevant aspects can be obtained by making the following approximating assumptions:

1) The flow is laminar and fully developed, which means the assumption of steady flow into a duct of rectangular cross-section which is long enough to be considered as open at its end.
2) The height of the channel D is small with respect to its width, W, so that the flow in the cavity can be approximated by the flow between two flat plates.
3) Melt front effects are neglected.
4) Transient effects are neglected.
5) Thermal properties are temperature independent.
6) The viscosity obeys the power-law:
$$\mu = \mu_0 \left(\frac{dv_z}{dx} \right)^{\nu - 1}$$
and is temperature-independent.
Here, μ, ν, v_z, and μ_0 denote the viscosity, power-law index, axial velocity, and consistency index, respectively.
7) Heat conduction in the flow direction is neglected.

Assumption 6) allows us to decouple the momentum and energy equations, which in our case read:

momentum: $$-\left(\frac{\partial P}{\partial z}\right)+\frac{\partial}{\partial x}\left(\mu\frac{\partial v_z}{\partial x}\right)=0 \qquad (1)$$

energy: $$\varrho c v_z(x)\frac{\partial T}{\partial z}=\lambda\frac{\partial^2 T}{\partial x^2}+\mu\left(\frac{\partial v_z}{\partial x}\right)^2 \qquad (2)$$

initial condition: $T=T_i$ for $z=0$

boundary conditions: $T=T_w$ at $x=D$ and $x=-D$ (isothermal wall),

where z denotes the axial coordinate, x the transverse coordinate, T the temperature, P the pressure, λ the thermal conductivity, and ϱc the specific heat per volume.

For convenience, we introduce the following dimensionless variables:

$$\tilde{T}=\frac{T-T_w}{T_i-T_w}\ ,\quad \tilde{x}=\frac{x}{D}\ ,\quad \tilde{z}=\frac{z}{L}\ ,\quad \tilde{v}_z=\frac{v_z}{\langle v_z\rangle}$$

$$Gz=\frac{\langle v_z\rangle D^2}{a\cdot L}\ ,$$

$$Br=\frac{\mu_0 D^2}{\lambda(T_i-T_w)}\left[\frac{(m+2)\langle v_z\rangle}{D}\right]^{(m+1)/m}\ ,$$

with $m=\frac{1}{\nu}$.

Two integrations of (1) and application of the non-slip and symmetry conditions yields the velocity profile for power law fluids:

$$\tilde{v}_z=\frac{m+2}{m+1}(1-|\tilde{x}|^{m+1})\ . \qquad (3)$$

After introduction into Eq. (2), the energy equation reads in dimensionless form:

$$\frac{m+2}{m+1}Gz(1-|\tilde{x}|^{m+1})\frac{\partial\tilde{T}}{\partial\tilde{z}}=\frac{\partial^2\tilde{T}}{\partial\tilde{x}^2}+Br\,|\tilde{x}|^{m+1} \qquad (4)$$

initial condition: $\tilde{T}=1$ for $\tilde{z}=0$,

boundary condition: $\tilde{T}=0$ at $\tilde{x}=\pm 1$.

The solution of the energy equation can be split up into a part independent of Br, $\tilde{T}_A$, and a part containing all dissipation effects, $Br\cdot\tilde{T}_B$:

$$\tilde{T}=\tilde{T}_A+Br\cdot\tilde{T}_B\ ,$$

with initial conditions $\tilde{T}_A(\tilde{z}=0)=1$,
$\tilde{T}_B(\tilde{z}=0)=0$

and boundary conditions $\tilde{T}_A(\hat{x}=0)=0$,
$\tilde{T}_B(\hat{x}=0)=0$.

Here, $\hat{x}$ denotes $1-|\tilde{x}|$. This can be expanded, giving for the energy Eq. (4):

$$(m+2)Gz\hat{x}\left[1-\frac{1}{2}m\hat{x}+\frac{1}{6}m(m-1)\hat{x}^2-\ldots\right]\frac{\partial\tilde{T}}{\partial\tilde{z}}$$
$$=\frac{\partial^2\tilde{T}}{\partial\hat{x}^2}+Br\left[1-(m+1)\hat{x}+\frac{1}{2}m(m+1)\hat{x}^2-\ldots\right]\ . \qquad (5)$$

Equation (4) can be solved with the method described in the appendix. In our case, the solution can be written as a function of the following similarity parameters (see also the appendix):

$$\chi\equiv\frac{(m+2)Gz\hat{x}^3}{9\tilde{z}}\ ,\quad \varepsilon\equiv\left(\frac{9\tilde{z}}{(m+2)Gz}\right)^{1/3}=\frac{\hat{x}}{\chi^{1/3}}\ . \qquad (6)$$

Applying the results derived in the appendix gives for the temperatures T_A and T_B:

$$\tilde{T}_A\simeq v_{A,0}(\chi)-\frac{\varepsilon m}{10}v_{A,1}(\chi)-\varepsilon^2[K_2 v_{A,2}(\chi)+K_3\chi^2 e^{-\chi}] \qquad (7A)$$

$$\tilde{T}_B\simeq\frac{1}{2}\varepsilon^2 v_{B,00}(\chi)-\frac{(m+1)}{6}\varepsilon^3 v_{B,10}(\chi)+\frac{m(m+1)}{18}\varepsilon^4 v_{B,20}(\chi)-\frac{(m+1)m(m-1)}{120}\varepsilon^5 v_{B,30}(\chi)+\frac{(m+1)m(m-1)(m-2)}{720}\varepsilon^6 v_{B,40}(\chi)\ . \qquad (7B)$$

This is, in fact, our final expression for the stationary temperature profiles including the viscous heating effect. The functions $v(\chi)$ are defined as:

$$v_{A,0}(\chi) = \frac{1}{\Gamma(1/3)}\gamma\left(\frac{1}{3},\chi\right)$$

$$v_{A,1}(\chi) = \chi^{1/3}\left[1-\frac{1}{\Gamma(4/3)}\gamma\left(\frac{4}{3},\chi\right)\right]$$

$$v_{A,2}(\chi) = \frac{\Gamma(5/3)}{\Gamma(4/3)}\chi^{1/3}e^{-\chi}\cdot M\left(\frac{5}{3},\frac{4}{3},\chi\right) - \frac{\Gamma(4/3)}{\Gamma(2/3)}e^{-\chi}\left[M\left(\frac{4}{3},\frac{2}{3},\chi\right)-2\chi-1\right]$$

$$v_{B,00}(\chi) = \frac{\Gamma(5/3)}{\Gamma(4/3)}\chi^{1/3}e^{-\chi}\cdot M\left(\frac{5}{3},\frac{4}{3},\chi\right)-\chi^{2/3}$$

$$v_{B,10}(\chi) = \frac{1}{\Gamma(4/3)}\chi^{1/3}e^{-\chi}\cdot M\left(2,\frac{4}{3},\chi\right)-\chi$$

$$v_{B,20}(\chi) = \chi^{1/3}$$

$$v_{B,30}(\chi) = \frac{\Gamma(8/3)}{\Gamma(4/3)}\chi^{1/3}e^{-\chi}\cdot M\left(\frac{8}{3},\frac{4}{3},\chi\right)-\chi^{5/3}$$

$$v_{B,40}(\chi) = \frac{2}{\Gamma(4/3)}\chi^{1/3}e^{-\chi}\cdot M\left(3,\frac{4}{3},\chi\right)-\chi^{2}$$

$$K_2 = \frac{\Gamma(2/3)}{\Gamma^2(4/3)}\cdot\frac{m(10-m)}{840}\,, \qquad K_3 = \frac{3m^2}{200\Gamma(4/3)}$$

and

$$\Gamma(4/3) = 0.8930\,, \qquad \Gamma(5/3) = 0.9027\,,$$

$$M(a,b,\chi) = \sum_{n=0}^{\infty}\frac{a(a+1)\ldots(a+n-1)\chi^n}{b(b+1)\ldots(b+n-1)n!}\,,$$

$$\gamma(a,\chi) = \frac{1}{a}\chi^a e^{-\chi}\cdot M(1,a+1,\chi)$$

denote two complete gamma functions, the Kummer function and the incomplete gamma function, respectively (see Abramowitz and Stegun 1972).

Note the $v_{A,1}$ and $v_{B,10}$ can be expressed in terms of $v_{A,0}$. The first term of Eq. (7B) equals Richardson's expression (1979) for the *Br*-dependent part of the solution. In Eq. (7B), all $v_{B,ki}$ terms with $i>0$ (as given in the appendix by Eq. (A20)) are neglected since the contribution of their sum turns out to be small. In physical terms this means that, for the viscous dissipation contribution, a linear velocity distribution in the convection part of the energy equation is assumed, whereas the source term is completely evaluated.

3. Comparison with core flow solution and numerical calculations

Core flow solution

Near $\hat{x}=1$, χ will be large since Gz is large. Therefore, the temperature in the core will not differ largely from its initial state and the dependence on χ is small. If the χ dependence is omitted, the solution of Eq. (4) reads:

$$\tilde{T}^{\text{core}}(\hat{x},\tilde{z}) = \tilde{T}_A^{\text{core}} + Br\cdot\tilde{T}_B^{\text{core}} = 1+\frac{Br\tilde{z}(1-\hat{x})^{m+1}}{Gz\left(\frac{m+2}{m+1}\right)\{1-(1-\hat{x})^{m+1}\}}\,. \quad (8)$$

In the limit of $\hat{x}\to 1$ Eq. (7) must yield Eq. (8). Indeed, using Eq. (A14) and $\varepsilon\chi^{1/3}=\hat{x}$, we obtain:

$$\tilde{T}(\varepsilon,\chi\to 1/\varepsilon^3) = 1-0(\varepsilon^2\chi^2e^{-\chi}) + \frac{Br\tilde{z}(1-\hat{x})^{m+1}}{Gz(m+2)\hat{x}}\{1+0(\chi^{-1})\}\,. \quad (9)$$

Thus, the *Br*-dependent part of Eq. (9) is the leading term of $\tilde{T}_B^{\text{core}}$.

Numerical calculations

In order to further check the validity of the analytical solution, a comparison is made with the numerical solution of Eq. (4) which was obtained by a finite difference technique based on Saul'yevs iteration scheme (see Pearson and Richardson 1983).

As a representative injection molding material PS DOW 678 is chosen with $\lambda = 0.13$ [W/mK], $a = 7\cdot10^{-8}$ [m^2/s], $\mu_0 = 6700$ [Pa·s$^{1/(1-m)}$], $m = 2.81$. In Table 1 all relevant injection molding conditions are summarized.

Table 1. Injection molding parameters

Figure	L [m]	W [m]	2D [mm]	T_i [°C]	T_w [°C]	$\langle v_z\rangle$ [m/s]	Gz	Br	Lit.
2	0.30	0.035	2.0	250	50	1.0	48	25.3	–
3	0.30	0.035	2.0	250	50	3.6	171	144	a)
4	0.20	0.050	2.0	256	56	1.15	82	30.8	b)

a) Van Wijngaarden et al. 1992
b Alles et al. 1986

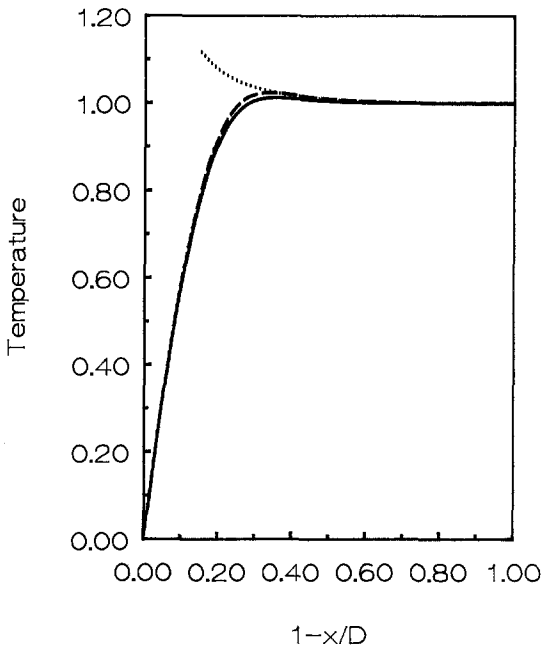

Fig. 2. Comparison of analytically predicted and numerically calculated dimensionless temperature profiles for $z/L = 0.25$, $Gz = 48$, $Br = 25.3$, and $m = 2.81$. The solid, dotted, and dashed lines represent the analytical, core flow, and the numerical solution of Eq. (4), respectively

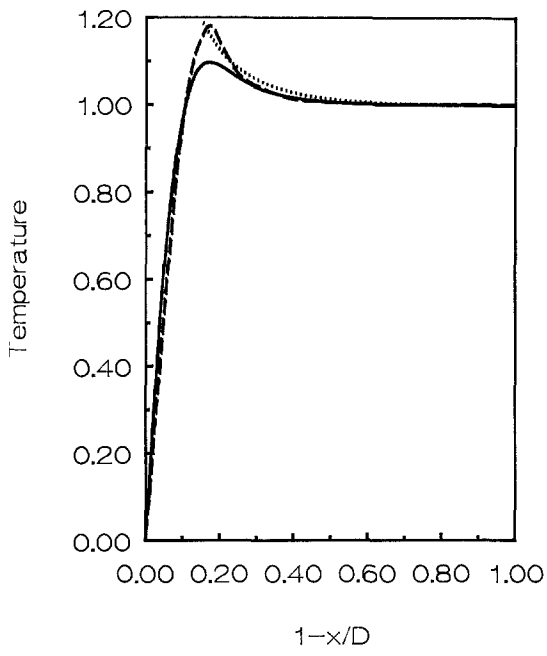

Fig. 3. Comparison of the dimensionless temperature profiles at the end of filling, predicted by the analytical approximation and the model used by Flaman 1990. The dimensionless quantities are: $z/L = 0.25$, $Gz = 171$, $Br = 144$, and $m = 2.81$. The solid, dotted, and dashed lines represent the analytical, core flow, and numerical predictions, respectively

In Fig. 2 the solution (7A, B) is compared with the numerical solution of Eq. (4) for a rather low Gz value of 48 and several axial positions. Near the mold wall, as well as in the mid-plane, the numerical and analytical solutions coincide, whereas the core flow solution joins both numerical and analytical solutions for $\hat{x} > 0.6$. The analytical solution underestimates the maximum temperature by about 1%. Still better predictions can be obtained for larger Gz numbers and smaller $\tilde{z}$ and Br values. We thus conclude the Eq. (7) is an accurate solution of the simplified model used.

More realistic models (Van Wijngaarden et al. 1982; Flaman 1990; Alles et al. 1986) also include unsteady effects, in particular, that flow is stopped when the mold is filled. These models use different, temperature-dependent constitutive equations. However, as will be shown below, near the duct entrance the temperatures predicted by those models agree surprisingly well with the model used in this paper.

The molding conditions as used by Van Wijngaarden et al. (1982) differ from those in Fig. 2. by a higher injection speed of 3.6 m/s. An extended version of their model was used by Flaman (1990) to calculate the temperatures indicated by the dashed line in Fig. 3. As can be seen from this figure, he

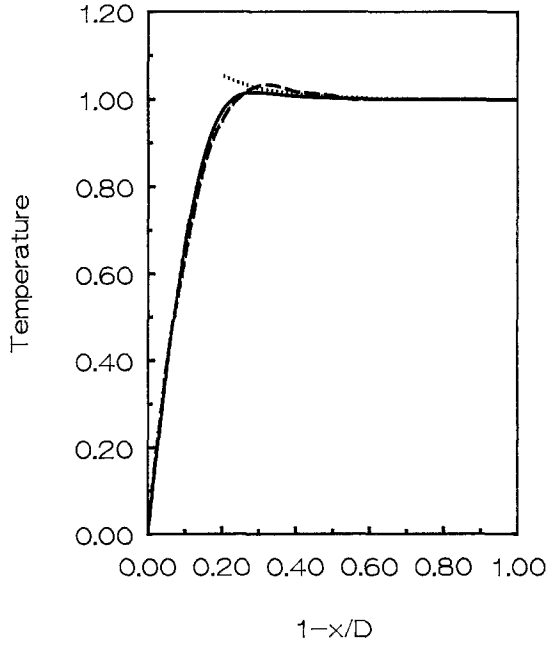

Fig. 4. Comparison of the dimensionless temperature profiles at the end of filling, predicted by the analytical approximation and the model used by Alles et al. 1986. The dimensionless quantities are: $z/L = 0.25$, $Gz = 82$, $Br = 30.8$, and $m = 2.81$

predicts an about 8% higher maximum temperature, whereas near the wall his calculated temperatures lie beneath the solution Eq. (7). This is due to the presence of the solidified layer which shifts the area where most viscous dissipation occurs towards the core. Since the frozen-in layer also decreases the effective cross-section, the velocity increases and more heat is dissipated. This will cause the viscosity to decrease. As is well-known, shearing is concentrated where the viscosity is lowered. In this way, the higher maximum of the curve obtained with Flaman's method can easily be explained. Alles et al. (1986) used experimentally determined viscosities in their numerical model to describe the filling process. In Fig. 4, we replotted the temperatures they calculated and added our predictions. Here, a similar trend as in Fig. 3 is seen. However, since Br is much smaller now, less heat is generated, resulting in a thicker solidified layer and a larger shift of the maximum towards the core.

4. Position of maximum temperature, solidified layer thickness, and simplified expressions

Position of the maximum temperature

An estimate of the position where the maximum temperature occurs, x_{max}, will now be made. We start with the leading term of T_A and the first three terms of T_B for large χ:

$$\tilde{T} \approx v_{A,0}(\hat{x}^3/\varepsilon^3) + \frac{\varepsilon^3 Br}{9}\left[\frac{1}{\hat{x}} - (m+1) + \frac{m(m+1)\hat{x}}{2}\right] .$$

After differentiation with respect to $\hat{x}$ and equating the derivative to zero, we find, as a first estimate of the position of the maximum,

$$\hat{x}_0 = \varepsilon \cdot \sqrt[3]{\ln (10/\varepsilon^4 Br)} .$$

Some improvement is gained by substituting $\hat{x}_1 = \hat{x}_0(1+\delta)$ and solving for δ. This results in a δ of about -0.1, while a direct comparison with numerical results leads to the same order of correction. Therefore, the position where the maximum temperature occurs is given by:

$$\hat{x}_{max} \approx 0.9\varepsilon \cdot \sqrt[3]{\ln (10/\varepsilon^4 Br)} . \qquad (10)$$

The absolute error in Eq. (10) is smaller than 0.01 for $\varepsilon^4 Br < 0.03$.

A simple expression of $\hat{x}_{max}$ for larger values of $\tilde{z}/Gz$ and Br, is not yet found.

Simplified expressions for the temperature profiles

Evaluation of the relative importance of the different order terms of T_A and T_B shows that, for $Gz = 0(100)$, the contribution of the second-order term to T_A is less than 0.01. Thus, for practical purposes a first-order approximation is sufficiently accurate. A good estimate of T_B can be obtained by considering only the first three terms, as given by (7B). To be more precise, an underestimation of at most $10^{-3} Br \cdot \tilde{z}$ is made for $Gz = 0(100)$.

In order to enhance calculation speed $v_{A,0}$, $v_{A,2}$, and $v_{B,00}$ can be fitted by the following simple expressions:

$$\tilde{v}_{A,0}(\chi) \approx 1 - (1 - 1.18\chi^{1/3} + 0.44\chi^{2/3}) e^{-\chi}$$
(absolute error ≤ 0.003)

$$\tilde{v}_{A,2}(\chi) \approx (0.71\chi^{0.25} + 1.2\chi) e^{-\chi}$$
(absolute error < 0.01) (11)

$$\tilde{v}_{B,00}(\chi) \approx \frac{2}{9}(1 - e^{-6.7\chi})\chi^{-1/3}$$
(absolute error < 0.01 for $\chi > 0.15$) .

Equation (8) gives the solution for large values of $\hat{x}$ ($\hat{x} > 0.2$), whereas Eq. (7) is especially suited for small $\hat{x}$. This suggests to try a hybrid form which matches $\tilde{T}_B$ for both small and large $\hat{x}$. Therefore, the trial function $(1 - \exp[-c\hat{x}^a \varepsilon^b])\tilde{T}_B^{core}$ is expanded for small $\hat{x}$ and compared with Eq. (7B). It then follows that the exponent becomes $-4.5\hat{x}^2/\varepsilon^2$. However, a somewhat smaller value of c appears to result in a better estimation of $\tilde{T}_B$ over the whole $\hat{x}$-region. We therefore write:

$$\tilde{T}_B \approx (1 - \exp[-2.9\hat{x}^2/\varepsilon^2]) \cdot \tilde{T}_B^{core} \qquad (12)$$
(absolute error $< 2 \cdot 10^{-4}$) .

Solidified layer thickness

For some purposes, for example, for a determination of the position of the boundary of the solidified layer, we need an expression for the isotherms. Therefore, we rewrite Eq. (7) as a series of ascending powers of $\hat{x}$ with coefficients which depend on ε. We then invert this series with the aid of the inversion equation listed by Abramowitz (1972) to obtain:

$$\hat{x}(\varepsilon, \tilde{T}) = \frac{\tilde{T}}{A} \frac{\left(\frac{m/\varepsilon}{10\Gamma(4/3)} - \frac{Br}{2}\right)\tilde{T}^2}{A^3}$$

$$+\frac{2\left(\dfrac{m/\varepsilon}{10\Gamma(4/3)}-\dfrac{Br}{2}\right)^2\cdot\tilde{T}^3}{A^5}$$

$$-\frac{Br(m+1)\tilde{T}^3}{6A^4}+0\left(\frac{\tilde{T}^4}{\varepsilon^4A^5}\right), \qquad (13)$$

where A is the first derivative of the temperature profile at the wall:

$$A=\frac{1}{\Gamma(4/3)\varepsilon}-\frac{m}{10}+\frac{Br\varepsilon}{2}\left(1-\frac{(m+1)\varepsilon}{3\Gamma(4/3)}\right). \qquad (14)$$

The solidification isotherm determines both the position and the magnitude of the frozen-in orientation peak (Wales 1972; Janeschitz-Kriegl 1979). Near the wall the temperature profile is almost linear and the first term of Eq. (13) is sufficient to describe the solidified layer thickness, $\hat{x}_{sol}$:

$$\hat{x}_{sol}=\frac{\tilde{T}_g}{A}, \qquad (15)$$

where $\tilde{T}_g$ denotes the dimensionless solidification temperature. In Fig. 5 the solidified layer thickness is given for the injection molding conditions of Fig. 3 with $\tilde{T}_g=0.25$ (solid line). The dashed line indicates the layer thickness without the dissipation contribution. It is clear that this contribution cannot be disregarded in our case. For the real case where flow stops when the mold is filled, it is interesting to know at which distance z from the entrance the analytical solution of this paper can no longer be considered as relevant. For this purpose also the predicted layer thickness of the penetration theory is shown. This line is obtained if only the residence time of the melt at the cold wall is taken into account, whereas convection is disregarded (see Janeschitz-Kriegl 1979).

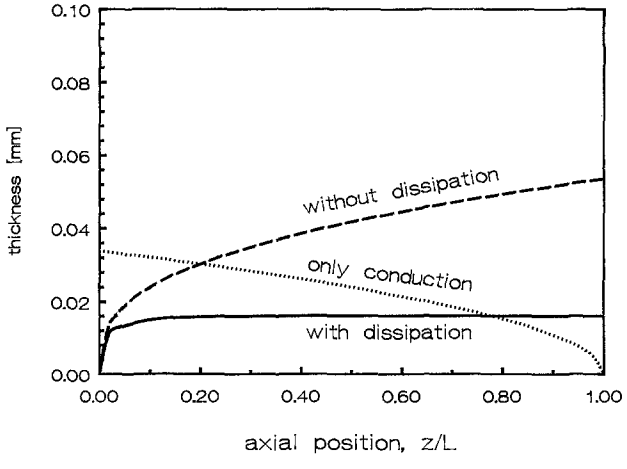

Fig. 5. Comparison of predicted, solidified layer thicknesses at the end of filling. The solid and dashed lines correspond to the conditions as used in Fig. 3 with $Br=144$ and $Br=0$, respectively. The dotted line is the layer thickness as predicted by the penetration theory, i.e., with $Gz=0$ and $Br=0$

5. Pipe flow solution

The method developed here for a rectangular mold can easily be extended to other geometries. As an example, a solution will be given for a cylindrical pipe. Let r denote the radial coordinate and z the axial coordinate in a circular pipe of radius R and length L. In this case, the dimensionless energy equation reads:

$$Gz\left(\frac{m+2}{m+1}\right)(1-\tilde{r}^{m+1})\frac{\tilde{T}}{\tilde{z}}=\frac{\partial^2\tilde{T}}{\partial\tilde{r}^2}+\frac{1}{\tilde{r}}\frac{\partial\tilde{T}}{\partial\tilde{r}}+Br\cdot\tilde{r}^{m+1} \qquad (16)$$

initial condition: $\tilde{T}=1$ for $\tilde{z}=0$

boundary condition $\tilde{T}=0$ at $\tilde{r}=1$,

where $\tilde{r}=r/R$. The treatment is very similar to the case treated before. On closer inspection, it turns out that the results of the channel flow solution, Eq. (7), can be used to obtain the solution for pipe flow (Richardson 1979):

$$\tilde{T}^{pipe}=\tilde{T}^{channel}-\frac{\hat{r}}{2}(1-v_{A,0})-\hat{r}^2\left(\frac{1}{4}+\frac{m}{20}\right)(1-v_{A,0})$$

$$-\varepsilon^2\left(\frac{1}{24}+\frac{m\chi}{20}\right)\frac{1}{\Gamma(4/3)}e^{-\chi}. \qquad (17)$$

The effect of the geometry on the T_B part is confined to the $v_{B,ki}$ terms with $i\geq 1$, which in our approach are not taken into account.

6. Conclusion

An analytical solution is presented for calculating the temperature profiles occurring in common injection molding circumstances. Situations with high injection speed, where the viscous heating is large, are also covered. A good agreement with the numerical solution for the region near the mold wall is found. Further, the solution is seen to converge to the asymptotic solution of the core flow.

Comparisons with some more extensive numerical models, as given in the literature (Flaman 1990; Alles et al. 1986), show differences of the relative temperatures of, at most, 8%. These differences are thought to be due to the assumptions which are made, such as temperature-independent viscosity.

The solution can be used to calculate the position of the maximum temperature and the solidification isotherms. Also, some approximate functions are derived to facilitate the calculation of the temperature field. Furthermore, an expression for the temperatures occurring in pipe flow are given.

Appendix: Perturbation solution of the diffusion equation

In this appendix a solution of the diffusion equation:

$$f(x)\frac{\partial T}{\partial z}=\frac{\partial^2 T}{\partial x^2}+g(x) \tag{A1}$$

initial condition: $T=h(x)$ for $z=0$

boundary conditions: $T=0$ at $x=0$ (A2)

and: $f(x)=f_0x^n(1+f_1x+f_2x^2+\ldots)$

$g(x)=g_0+g_1x+g_2x^2+\ldots$

$h(x)=h_0+h_1x+h_2x^2+\ldots$

is sought for small x. For convenience, the $g(x)$ part will be separated from the partial differential equation by introducing $T=T_A+T_B$, where T_A is the solution of the homogeneous equation. T_A satisfies the boundary and initial conditions (A2). T_B is the solution of (A1) with $T_B(x=0)=0$ and $T_B(z=0)=0$ as boundary and initial conditions, respectively.

A similarity solution is tried by introducing the parameters ε and χ, so that T_A can be expanded in a series of powers of the small parameter ε:

$$\varepsilon\equiv\left(\frac{(n+2)^2z}{f_0}\right)^{1/(n+2)},\quad \chi\equiv\left(\frac{x}{\varepsilon}\right)^{n+2}=\frac{f_0x^{n+2}}{(n+2)^2z},$$

$$T_A=\sum_{k=0}^{\infty}\varepsilon^k\cdot\vartheta_{A,k}(\chi)\ . \tag{A3}$$

After performing all substitutions and equating equal powers of ε, an inhomogeneous Kummer differential equation (Abramowitz and Stegun 1972) results for each $\vartheta_{A,k}$:

$$\chi\ddot{\vartheta}_{A,k}+\left(\frac{n+1}{n+2}+\chi\right)\dot{\vartheta}_{A,k}-\frac{k}{n+2}\vartheta_{A,k}$$

$$=-\sum_{i=1}^{k}f_i\chi^{i/(n+2)}\left(\chi\dot{\vartheta}_{A,k-i}-\frac{k-i}{n+2}\vartheta_{A,k-i}\right) \tag{A4}$$

with $\vartheta_{A,k}(0)=0$, $\vartheta_{A,k}(\chi\to\infty)=h_k\chi^{k/(n+2)}$,

where $\dot{}$ stands for differentiation with respect to χ.

Note that the introduction of χ implies that the initial situation is not only reached for small values of z, but also for large x.

For $k=0$ the inhomogeneous part of Eq. (A4) equals zero and the solution of $\vartheta_{A,0}(\chi)$ is easily obtained:

$$\vartheta_{A,0}(\chi)=\frac{h_0}{\Gamma\left(\frac{1}{n+2}\right)}\gamma\left(\frac{1}{n+2},\chi\right)\ , \tag{A5}$$

where $\gamma(a,\chi)$ denotes the incomplete gamma function defined as

$$\gamma(a,\chi)=\int_0^{\chi}t^{a-1}e^{-t}dt\ .$$

For $k>0$, the inhomogeneous part of Eq. (A4) turns out to be of the form $K\chi^qe^{-\chi}$. Buchholz (1953) proves that the differential equation

$$\chi\ddot{\vartheta}+(b+\chi)\dot{\vartheta}-a\vartheta=K\chi^qe^{-\chi}$$

has the particular solution:

$$\vartheta_{\text{part}}=\frac{K\chi^{q+1}e^{-\chi}}{(q+b)(q+1)}$$

$$\cdot{}_2F_2(1,q+a+b+1;q+b+1,q+2;\chi)\ , \tag{A6}$$

where ${}_2F_2(1,a;b,c;\chi)$ is a generalized hypergeometric function defined as ${}_2F_2(1,a;b,c;\chi)=\sum_{k=0}^{\infty}\frac{(a)_k\chi^k}{(b)_k(c)_k}$, and $(a)_k$ denotes Pochammer's symbol: $(a)_k=a(a+1)\ldots(a+k-1)$.

Using this solution together with the homogeneous solutions, we can calculate the next two terms of T_A:

$$\vartheta_{A,1}(\chi)=\frac{f_1h_0}{n+4}v_{A,1}(\chi)+h_1\chi^{1/(n+2)} \tag{A7}$$

$$\vartheta_{A,2}(\chi) = (h_2 - K_2)\, v_{A,21}(\chi) + K_2 v_{A,22}(\chi) - K_3 \chi^{(n+5)/(n+2)} e^{-\chi} , \tag{A8}$$

where $K_2 = \dfrac{3\,\Gamma\left(\frac{2}{n+2}\right)\Gamma\left(\frac{3}{n+2}\right)}{2(n+6)\cdot\Gamma\left(\frac{1}{n+2}\right)\Gamma\left(\frac{4}{n+2}\right)} h_0 \cdot \left[\frac{(n+5)f_1^2}{2(n+4)} - f_2\right]$,

$$K_3 = \frac{h_0 f_1^2}{2\left(\frac{n+4}{n+2}\right)^2 \cdot \Gamma\left(\frac{1}{n+2}\right)} ,$$

$$v_{A,1}(\chi) = \chi^{1/(n+2)} \left[1 - \frac{1}{\Gamma\left(\frac{n+3}{n+2}\right)} \cdot \Gamma\left(\frac{n+3}{n+2}, \chi\right)\right]$$

$$v_{A,21}(\chi) = \frac{2\Gamma\left(\frac{2}{n+2}\right)}{\gamma\left(\frac{1}{n+2}\right)} \chi^{1/(n+2)} e^{-\chi} \cdot M\left(\frac{n+4}{n+2}, \frac{n+3}{n+2}, \chi\right)$$

$$v_{A,22}(\chi) = \frac{\Gamma\left(\frac{4}{n+2}+2\right)}{\Gamma\left(\frac{3}{n+2}+2\right)\Gamma\left(\frac{2}{n+2}+2\right)} \chi^{(n+5)/(n+2)} e^{-\chi} \cdot {}_2F_2\left(1, \frac{4}{n+2}+2; \frac{3}{n+2}+2, \frac{2}{n+2}+2; \chi\right) .$$

The contribution of T_B can be found in a manner similar to the calculation of T_A. The asymptotic solution for large values of x, T_B^{as} can be obtained by letting $\partial T_B/\partial x$ in Eq. (A1) vanish:

$$T_B^{as}(x \to \infty, z) = \frac{g(x)\cdot z}{f(x)} . \tag{A9}$$

The introduction of χ according to Eq. (A3) implies that this solution has also to apply for small values of z. In this case the right-hand side of Eq. (A9) vanishes, which is consistent with the initial condition. Further, a slightly different perturbation series is introduced: $T_B = \varepsilon^2 \sum_{k=0}^{\infty} \varepsilon^k \vartheta_{B,k}(\chi)$. This results in the following set of differential equations:

$$\chi \ddot{\vartheta}_{B,k} + \left(\frac{n+1}{n+2} + \chi\right)\dot{\vartheta}_{B,k} - \frac{k+2}{n+2}\vartheta_{B,k} = -\frac{g_k}{(n+2)^2}\chi^{(k-n)/(n+2)} - \sum_{i=1}^{k} f_i \chi^{1/(n+2)} \cdot \left(\chi \dot{\vartheta}_{B,k-1} - \frac{k-i+2}{n+2}\vartheta_{B,k-i}\right) , \tag{A10}$$

with

$$\vartheta_{B,k}(\chi = 0) = 0 ,$$

$$\varepsilon^2 \sum_{k=0}^{\infty} \varepsilon^k \vartheta_{B,k}(\chi \to \infty, \varepsilon = 0) = T_B^{as}(x, 0) = 0 . \tag{A11}$$

In fact, the initial condition turns out to be such that each $\vartheta_{B,k}$ vanishes for large χ.

The homogeneous solutions are similar to those of $\vartheta_{A,k}$, whereas the particular solution can be considered to consist of two parts, one resulting from the first term and the other from the last term on the right-hand side of (A10). The first part can easily be found. As can be verified by substitution, this reads:

$$\vartheta_{B,\text{part}\,1}(\chi) = -\frac{g_k}{(k+1)(k+2)} \chi^{(k+2)/(n+2)} .$$

Applying the initial and boundary condition now yields:

$$\vartheta_{B,k0}(\chi) = \frac{g_k}{(k+1)(k+2)} \cdot v_{B,k0}(\chi) , \tag{A12}$$

where

$$v_{B,k0}(\chi) = \frac{(k+2)\,\Gamma\left(\frac{k+2}{n+2}\right)}{\Gamma\left(\frac{1}{n+2}\right)} \chi^{1/(n+2)} e^{-\chi} \cdot M\left(\frac{k+2}{n+2}+1, \frac{n+3}{n+2}, \chi\right) - \chi^{(k+2)/(n+2)} \tag{A13}$$

$$v_{B,k0}(\chi\to\infty)=\left(\frac{k+1}{n+2}\right)\left(\frac{k+2}{n+2}\right)\cdot\chi^{(k-n)/(n+2)}. \tag{A14}$$

The particular solution due to the last term of (A9) can be found by expanding the $\vartheta_{B,k-1}$ solutions in powers of χ, multiplied by $\exp(-\chi)$. Using (A6), this results in a particular solution consisting of a series of ${}_2F_2(1,a;b,c;\chi)$ functions, which will be denoted as $G_{ki}(\chi)$:

$$G_{ki}(\chi)\equiv\chi^{(i+n+3)/(n+2)}e^{-\chi}\cdot\sum_{r=0}^{\infty}\frac{\left(\frac{k-i+2}{n+2}\right)_r\chi^r\,{}_2F_2\left(1,\frac{k+i+2}{n+2}+r+2;\frac{i}{n+2}+r+2,\frac{i+1}{n+2}+r+2;\chi\right)}{\left(\frac{n+3}{n+2}\right)_r r!\left(\frac{i+n+2}{n+2}+r\right)\left(\frac{i+n+3}{n+2}+r\right)}. \tag{A15}$$

In order to apply the initial conditions, we must know the asymptotic behavior of G_{ki}. This turns out to be:

$$G_{ki}(\chi\to\infty)=S_{ki}\cdot\chi^{(k+2)/(n+2)}, \tag{A16}$$

with

$$S_{ki}=\frac{\Gamma\left(\frac{i+n+2}{n+2}\right)\Gamma\left(\frac{i+n+3}{n+2}\right)}{\Gamma\left(\frac{k+i+2}{n+2}+2\right)}\cdot{}_3F_2\left(\frac{k-i+2}{n+2},\frac{i+n+2}{n+2},\frac{i+n+3}{n+2};\frac{n+3}{n+2},\frac{k+i+2}{n+2}+2;1\right). \tag{A17}$$

Thus, the final expression for T_B becomes:

$$T_B=\sum_{k=0}^{\infty}\varepsilon^{k+2}\cdot\left\{\frac{g_k}{(k+1)(k+2)}v_{B,k0}(\chi)+\sum_{i=1}^{k}\vartheta_{B,ki}(\chi)\right\}, \tag{A18}$$

where

$$\vartheta_{B,ki}(\chi)=C_{ki}\cdot S_{ki}\cdot v_{B,ki}(\chi)\ ,\quad \text{for}\quad i>0 \tag{A19}$$

$$v_{B,ki}(\chi)=-\left[\frac{\Gamma\left(\frac{k+2}{n+2}+1\right)}{\Gamma\left(\frac{n+3}{n+2}\right)}\chi^{1/(n+2)}e^{-\chi}\cdot M\left(\frac{k+2}{n+2}+1,\frac{n+3}{n+2},\chi\right)-\frac{G_{ki}(\chi)}{S_{ki}}\right],\quad i>0, \tag{A20}$$

and

$$C_{ki}=\frac{f_i g_{k-i}}{(n+2)^2}\cdot\frac{\Gamma\left(\frac{k-i+2}{n+2}\right)}{\Gamma\left(\frac{n+3}{n+2}\right)}.$$

Acknowledgement

The numerical calculations leading to Fig. 3, were performed by A. A. M. Flaman of the Philips Research Laboratories, The Netherlands.

References

Abramowitz M, Stegun IA (1972) Handbook of mathematical functions. Dover, New York

Alles H, Philipon S, Agassant JF, Vincent M (1986) Experimental and theoretical study of the filling stage of a rectangular plaque: application to a spiral mold. Pol Proc Eng 4:71–96

Buchholz H (1953) Die Konfluente Hypergeometrische Funktion. Springer, Berlin, p 37

Flaman AAM (1990) Build-up and relaxation of molecular orientation in injection moulding. PhD Thesis, Eindhoven Technical Univ

Janeschitz-Kriegl H (1979) Injection moulding of plastics. II Analytical solution of heat transfer problem. Rheol Acta 18:693–701

Lévêque MA (1928) Les lois de la transmission de la chaleur par convection. Ann Mines 13:201, 305, 381

Newman J (1969) Extension of the Lévêque solution. J Int Heat Transfer 91:177–178

Pearson JRA (1985) Mechanics of polymer processing. Ch 19: Injection moulding. Elsevier Appl Sci Publ, London

Pearson JRA, Richardson SM (1983) Computational analysis of polymer processing. Applied Science Publ, London

Richardson SM (1979) Extended Lévêque solutions for power law fluids in pipes and channels. Int J Heat Mass Transfer 22:1417 – 1423

Richardson SM (1983) Injection moulding of thermoplastics: freezing during mould filling. Rheol Acta 22:223 – 236

Ryan ME, Chung TS (1980) Conformal mapping analysis of injection mold filling. Pol Eng Sci 20:642 – 651

Van Wijngaarden H, Dijksman JF, Wesseling P (1982) Non-isothermal flow of a molten polymer in a narrow rectangular cavity. J Non-Newtonian Fluid Mech 11:175 – 199

Wales JLS (1972) Some aspects of orientation in injection moulded objects. Pol Eng Sci 12:358 – 363

(Received February 3, 1992;
in revised form May 26, 1992)

Correspondence to:

K.M.B. Jansen
Department of Polymer Technology
Delft University of Technology
P.O.Box 5045
2600 GA Delft
The Netherlands